Migration of radionuclides in a gas cooled solid state spallation target

Jørgensen, Thomas; Severin, Gregory; Jensen, Mikael

Published in:
Nuclear Engineering and Design

Link to article, DOI:
10.1016/j.nucengdes.2014.10.021

Publication date:
2015

Document Version
Peer reviewed version

Migration of Radionuclides in a Gas Cooled Solid State Spallation Target

Thomas Jørgensen[a], Gregory Severin[a], Mikael Jensen[a,*]

[a]*Hevesy Lab, Nutech, Risoe-DTU,Technical University of Denmark, DK-4000 Roskilde, Denmark*

Abstract

The current design of the ESS (European Spallation Source) program proposes a rotating solid tungsten target cooled by helium gas and a pulsed beam of protons. For safety reasons any design has to address wether or not the induced radionuclidic isotopes in the target move.

In this paper we have investigated the diffusion of (primarily) Tritium in solid tungsten to see, if a pulse driven short-term variation in temperature (temperature peaks separated by one turn of the wheel (2.36 secs)) could possibly give rise to wave-like migration of the radionuclides, possibly accelerating the overall release.

In order to calculate the diffusion in the solid tungsten target two approaches have been used. One neglecting the time structure of the beam and thermal cycling of the target, and one numerical, discrete time step simulation to capture the effects of the thermal cycling on the diffusion behavior.

We found that the time structure of the of the temperature has a negligible impact on the diffusion, and that the radioactive release at the surface can be calculated safely by solving the differential equation (Fick's law) using an appropriate temperature to calculate the diffusion constant.

Keywords: Spallation Target, Safety, Tritium

1. Introduction

The uses of spallation as a source of neutrons for materials studies, isotope production, subcritical reactor operation and waste transmutation are well

*email: kmje@dtu.dk

known and documented [1]. As proton energy increases, the neutron yield per incident proton increases, however a practical plateau of neutron yield per beam power unit delivered to the target is reached in the region 1-2.5 GeV. State of the art and projected future spallation sources all use proton drivers in this range (ISIS, SNS, JPARC, ESS). As accelerator technology and capability increases, an obvious improvement to neutron source output is obtained by increase in beam power.

On the other hand, target integrity and safety are fundamental limits to the beam power that can be deposited. The main obstacles to higher power are target cooling and radiation damage, but equally important is the need to contain and control the induced activity in the target because of operability, facility safety and environmental concerns. The spectrum of induced radioactive isotopes depends of course on the target material, but all spallation sources have a common load of potential dangerous radioisotopes, which have to be contained.

Liquid metal targets and especially mercury targets have been a viable technical solution to high power targets in the 1-2 MW range (SNS, JPARC). The benefit of the liquid metal is the possibility of cooling by circulation and the self annealing properties of the liquid, preventing build up of radiation damage. However, early experimental findings [2] and later detailed computational and experimental analysis [3] have identified the "cavitation pinching" problem on the stainless steel surfaces exposed to the liquid mercury in the high power beam.

Prudent material choices, cooling conditions and beam conditioning have shown to alleviate this problem to the necessary extent at SNS. At time of target design at ESS, it was however seen as a safer approach to power levels above 2 MW to use a solid target. In addition, the liquid metals pose problems to both target material and radioisotope containment because of the chemical nature of the major radioisotopes induced (polonium isotopes from bismuth, mercury isotopes from mercury target).

The current ESS design is a compromise between the best obtainable neutron source brilliance (interaction length), pulse duration (energy dispersity) and radioisotope containment. The compromise is a solid tungsten target consisting of centimeter to decimeter size slabs in a rotating geometry and cooled by high velocity stream of helium gas [4].

The ultimate radiological safety and operability of this design depends on a restriction of mobility of all the important radioisotopes. This again depends on the mechanical integrity of the target material (tungsten kept well

below the melting point), but also on the diffusion behavior of the various radioelements in tungsten as well as the surface behavior in the interface to the cooling helium. By nature the gas cooling loop is a rapid and highly efficient transport mechanism for any isotope capable of going into the gas phase at the target surface.

This paper focuses on the first part of the transport problem, the possible diffusion in the target. This is only a partially explored field, as normal trace element diffusion in tungsten might be known or calculable, while the knowledge of radiation damage enhanced diffusion is very limited. As an attempt to solve the first part of the problem we have investigated two approaches to the diffusion, one neglecting the time structure of the beam and thermal cycling of the target, while the other method is an attempt by numerical, discrete time step simulation to capture the effects of the thermal cycling on diffusion behavior.

By the usage of mathematical modeling, we include combined solutions of the heat and diffusion equations together with the radioactive decay law under conditions of spatial and temporal varying production rate on a tungsten spallation target.

2. Material and methods

2.1. General aspects of the model

In principal, all the different shapes and position of target blocks should be modeled. The azimuthal positions of the blocks are completely symmetrical, but geometry, heat load and beam profile differ greatly with depth in the target.

However, it is the front blocks (the outer rim of the wheel) that experience the highest heat load and the highest radionuclide production and concentrations. For this reason we have concentrated on the behavior of the foremost front block in the proposed tungsten target wheel in the work of this paper.

This block not only serves as a good model system to compare our analytical and numerical approach, but the results can also be used to provide a conservative and safe limit to total radionuclide release, if the results from the front block are scaled by the ratio between the total radionuclide inventory and front block inventory.

2.2. Analytical solution

Diffusion of impurities through materials obeys first order kinetics following Fick's law,

$$\frac{\partial \phi}{\partial t} = D\nabla^2\phi \tag{1}$$

where ϕ is the local concentration of the diffusing impurity.

For species with active chemical removal occurring at the material surface, the boundary condition becomes

$$\phi|_{boundary} = 0 \tag{2}$$

The solution to Fick's law with such boundaries on a three dimensional rectangular block is separable

$$\phi(\vec{x}, t, t') = \sum_{l,m,n} X_{l,m,n}(\vec{x}) T_{l,m,n}(t, t') \tag{3}$$

with solutions of the form:

$$X_{l,m,n}(\vec{x}) = A_l B_m C_n \sin\frac{l\pi x}{L_x} \sin\frac{m\pi y}{L_y} \sin\frac{n\pi z}{L_z} \tag{4}$$

and

$$T_{l,m,n}(t, t') = e^{-D\pi^2(t-t')[\frac{l^2}{L_x^2}+\frac{m^2}{L_y^2}+\frac{n^2}{L_z^2}]} \tag{5}$$

Where A_l, B_m, C_n are Fourier coefficients with the form

$$A_l = \frac{2}{L_x}\int_0^{L_x} f(x)\sin(\frac{l\pi x}{L_x}) \tag{6}$$

derived from the input concentration function, $M(\vec{x})$, defined as

$$M(\vec{x}) = f(x)g(y)h(z) = \phi(\vec{x}, t', t') \tag{7}$$

Here f, g, h are the one-dimensional input distributions, and n, l, m are indexes for the x, y, and z solutions respectively. L's are the x, y and z lengths of the rectangular block, D is the diffusion coefficient, and t' is the input time.

For the case of beam-induced particle creation, impurities are generated at a rate, R, with the distribution $\phi(\vec{x}, t', t)$. Integrating this over input

times, t' from beam-on, t_0, to time t, weighted by radioactive decay, gives the local impurity concentration as a function of time, $\Phi(\vec{x}, t)$:

$$\Phi(\vec{x}, t) = \int_{t_0}^{t} R\,\phi(\vec{x}, t', t)\, e^{-\lambda(t-t')}\, dt' \tag{8}$$

where λ is the radioactive decay constant. Evaluation of this integral gives

$$\Phi(\vec{x}, t) = \sum_{l,m,n} \frac{R\, X_{l,m,n}(\vec{x})}{\lambda + D\pi^2(\frac{l^2}{L_x^2} + \frac{m^2}{L_y^2} + \frac{n^2}{L_z^2})} \left(1 - T_{l,m,n}(t, t_0) e^{-\lambda(t-t_0)}\right) \tag{9}$$

Further, spatial integration over the entire block gives the total activity in the block as a function of time, $\Theta(t, t_0)$,

$$\Theta(t, t_0) = \sum_{l,m,n} \frac{8R\, L_x L_y L_z A_l B_m C_n \left(1 - T_{l,m,n}(t, t_0) e^{-\lambda(t-t_0)}\right)}{\pi^3 lmn \left[\lambda + D\pi^2(\frac{l^2}{L_x^2} + \frac{m^2}{L_y^2} + \frac{n^2}{L_z^2})\right]} \tag{10}$$

The x, y functional form of $M(\vec{x})$ is defined by the ESS beam-strike, given in the Baseline Specification. From there, a safe assumption is uniform isotope production in z. Therefore

$$f(x) = \frac{3}{4\Delta_x} \left[1 - \frac{(x - L_x/2)^2}{\Delta_x^2}\right] \tag{11}$$

$$g(y) = \frac{3}{4\Delta_y} \left[1 - \frac{(y - L_y/2)^2}{\Delta_y^2}\right] \tag{12}$$

and

$$h(z) = 1/L_z \tag{13}$$

where Δ_x and Δ_y are parameters determining the beam width.

Evaluation of the Fourier integrals (eg. 6) for these distributions gives

$$A_l = \frac{-6L_x}{(l\pi\Delta_x)^2} \left[\sin\left(l\pi(\frac{1}{2} + \frac{\Delta_x}{L_x})\right) + \frac{L_x}{\Delta_x l\pi} \cos\left(l\pi(\frac{1}{2} + \frac{\Delta_x}{L_x})\right)\right] \tag{14}$$

$$B_m = \frac{-6L_y}{(m\pi\Delta_y)^2} \left[\sin\left(m\pi(\frac{1}{2} + \frac{\Delta_y}{L_y})\right) + \frac{L_y}{\Delta_y m\pi} \cos\left(m\pi(\frac{1}{2} + \frac{\Delta_y}{L_y})\right)\right] \tag{15}$$

and

$$C_n = \frac{4}{n\pi L_z} \tag{16}$$

when $n, l, m = odd$. A_l, B_m, C_n are zero for $n, l, m = even$ respectively.

For the simplified case of $\Delta_x = L_x/2$ and $\Delta_y = L_y/2$ the expression $\Theta(t, t_0)$ becomes

$$\Theta(t, t_0) = \sum_{l,m,n=odd} \frac{73728R\left(1 - T_{l,m,n}(t, t_0)e^{-\lambda(t-t_0)}\right)}{\pi^{10}l^4m^4n^2\left[\lambda + D\pi^2(\frac{l^2}{L_x^2} + \frac{m^2}{L_y^2} + \frac{n^2}{L_z^2})\right]} \tag{17}$$

From eq.17, it is clear that the $l = m = n = 1$ term is dominant, and roughly 79% of all radioactive impurities populate this state. Additionally, it is apparent that all states saturate with their respective time constant, $\lambda^*_{l,m,n}$

$$\lambda^*_{l,m,n} = \lambda + \lambda_{l,m,n} \tag{18}$$

where

$$\lambda_{l,m,n} = D\pi^2(\frac{l^2}{L_x^2} + \frac{m^2}{L_y^2} + \frac{n^2}{L_z^2}) \tag{19}$$

The release rate constant from the target due to diffusion, λ_d is therefore

$$\lambda_d = \sum_{l,m,n=odd} \frac{0.787}{l^4m^4n^2}\lambda_{l,m,n} \tag{20}$$

for this example, or

$$\lambda_d = \sum_{l,m,n=odd} \frac{8A_lB_mC_nV}{lmn\pi^3}\lambda_{l,m,n} \tag{21}$$

for the general case, where V is the volume of the rectangular block. The rate constant (λ_d) represents the overall, volume integrated diffusion constant for a given block. The dimension of λ is time^{-1} and $\frac{1}{\lambda}$ is the typical time, t_d for release of a given species of activity.

2.3. Numerical solution

In order to make the numerical calculations we need a 3D mesh of cubes. Since the curvature for the outermost blocks of the target is negligible, we use cartesian geometry. Figure 1 shows the geometry for such a block.

The block is divided into unit cells of 1 mm^3, and the net energy flow rate and the net diffusion flow rate of each cell are then used to calculate the temperature change and the concentration change in every cell. This is done in time steps Δt for a number of pulses.

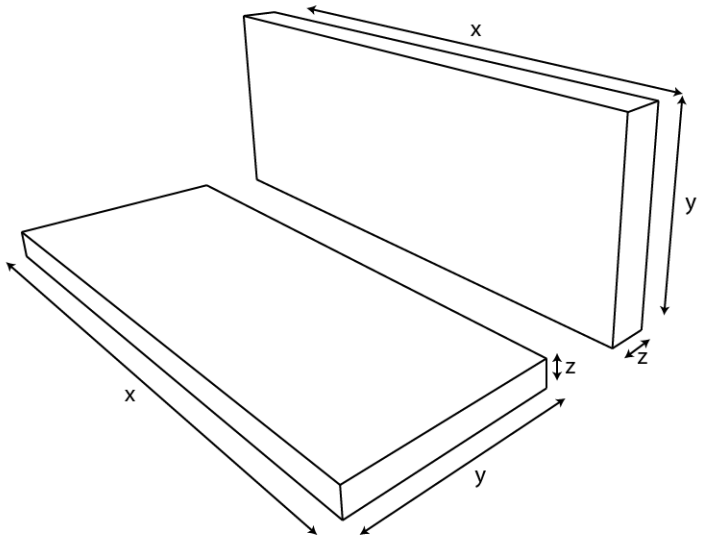

Figure 1: The figure shows a sketch of the tungsten block with x,y and z directions denoted. $x = 120\,\mathrm{mm}, y = 80\,\mathrm{mm}$ and $z = 13\,\mathrm{mm}$.

2.3.1. Temperature

The numerical approach allows a more detailed description of the small scale variances in space and time of the instantaneous diffusion coefficient inside the tungsten blocks. From earlier simulations in the target design update process [5], the temperatures on the surface of the tungsten block vary from all most inlet temperature to about 550°C, depending on position along beam path and on position relative to beam profile.

The temporal variation reflects revolution of the target wheel, designed in such a way that only one beam pulse hits a given block per revolution. (We ignore the rf-microstructure of the beam).

We have used the frontmost tungsten block to calculate the temperature profiles and time variation, because this block sees the highest power density. We assume an inlet temperature of the helium of constant 25°C. We distribute the total helium mass flow rate of 3 kg/sec over the total flow cross section surface area of the target, which is 0.17 m^2. This gives a mass velocity, $G = 3\,\frac{\mathrm{kg}}{\mathrm{s}}/0.17\,\mathrm{m}^2 = 17.65\,\mathrm{kg}/(\mathrm{m}^2 \cdot \mathrm{s})$.

The heat transfer coefficient to the He gas can be found from the following

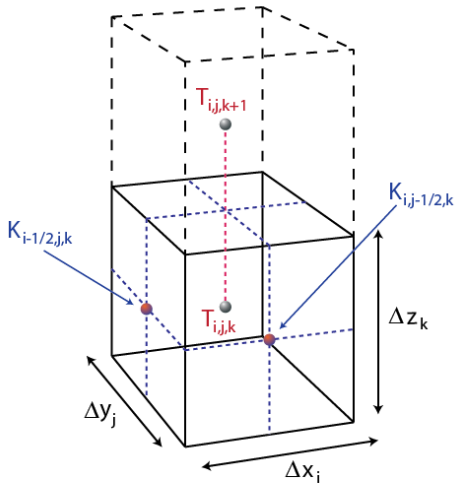

Figure 2: Unit cells (i, j, k) and $(i, j, k + 1)$. K's are the thermal conductances connected to the cell (i, j, k), which will be the same in this case.

relation [6]:

$$\frac{hD_e}{k} \simeq 0.020 \cdot Re^{0.8}$$

where D_e is the equivalent diameter of the gas flow, k is the heat conduction coefficient for the He gas and Re is Reynolds number. This gives a heat transfer coefficient of 484 W/(m^2·K).

Using this and a thermal conductivity of tungsten equal to value of 173 W/(m·K) (taken at 20°C), we can calculate the time course of temperature of each unit cell inside the front tungsten block. For this we have used the beam profile that is described by a normalized parabolic expression [4]:

$$z = C\frac{9}{16AB}\left(1 - \frac{x^2}{A^2}\right)\left(1 - \frac{y^2}{B^2}\right) \tag{22}$$

where C is a normalizing constant chosen in such a way that the peak of the profile has a value of 3.3 kW/cm^3, since the beam power average is 5 MW. $A = 80$ mm is half the width and $B = 30$ mm is half the hight of the beam footprint.

The energy flow rate from cell (i, j, k) to cell $(i, j, k + 1)$ is calculated as:

$$P_{i,j,k+\frac{1}{2}} = K_{i,j,k+\frac{1}{2}}(T_{i,j,k+1} - T_{i,j,k}) \tag{23}$$

where $K_{i,j,k+\frac{1}{2}}$ is the thermal conductance between the two cells, which can be found as:

$$K_{i,j,k+\frac{1}{2}} = \frac{\lambda_{i,j,k}A}{\Delta z_k} = \frac{\lambda_{i,j,k}\Delta x_i \Delta y_j}{\Delta z_k} \tag{24}$$

$\lambda_{i,j,k}$ is the thermal conductivity in cell (i, j, k), which is that of tungsten, $\lambda_W = 173$ (W/(m·°C)), A is the area of the facet between cell (i, j, k) and $(i, j, k+1)$, Δz_k is the distance (m) between the centers of the two cells. $T_{i,j,k}$ and $T_{i,j,k+1}$ are the temperatures in the two cells.

The total energy flow rate through the 6 facets of the cube cell inside the block is then described by:

$$\begin{aligned} P_{total(i,j,k)} = {} & K_{i-\frac{1}{2},j,k}(T_{i-1,j,k} - T_{i,j,k}) + K_{i+\frac{1}{2},j,k}(T_{i+1,j,k} - T_{i,j,k})... \\ & + K_{i,j-\frac{1}{2},k}(T_{i,j-1,k} - T_{i,j,k}) + K_{i,j+\frac{1}{2},k}(T_{i,j+1,k} - T_{i,j,k})... \\ & + K_{i,j,k-\frac{1}{2}}(T_{i,j,k-1} - T_{i,j,k}) + K_{i,j,k+\frac{1}{2}}(T_{i,j,k+1} - T_{i,j,k}) \end{aligned} \tag{25}$$

The cells in the boundary layer of the tungsten block have 1-3 facets facing the He gas. The energy flow rate through these facets (facing the He gas) is given by (e.g. for cell $(1, j, k)$):

$$P = hA(T_{He} - T_{i,j,k}) \tag{26}$$

where h is the heat transfer coefficient at the surface from tungsten to the He gas (found above), A is the area of the facet, T_{He} is the temperature of the He gas (which is assumed to be constant) and $T_{1,j,k}$ is the temperature of the cell. The energy flow rate through the rest of the facets is described in the same way as in eq. 25.

This causes a change of equation 24 for the boundary cells. Again we look at cell $(1, j, k)$. The conductance that couples the temperature of the cell with the boundary temperature (temperature of He gas) is:

$$K_{\frac{1}{2},j,k} = \frac{\Delta y_j \Delta z_k}{\Delta x_1/(2\lambda_{1,j,k}) + 1/h} \tag{27}$$

The first term in the denominator is the thermal resistance in the x-direction for half the cell $(1, j, k)$ and the second term is the resistance in the interface to the He gas.

Hence, the total energy flow rate through the unit cell $(1, j, k)$ with only one facet facing the He gas is:

$$\begin{aligned} P_{total(1,j,k)} = K_{\frac{1}{2},j,k}(T_{He} - T_{1,j,k}) + K_{\frac{3}{2},j,k}(T_{2,j,k} - T_{1,j,k})... \\ + K_{1,j-\frac{1}{2},k}(T_{1,j-1,k} - T_{1,j,k}) + K_{1,j+\frac{1}{2},k}(T_{1,j+1,k} - T_{1,j,k})... \\ + K_{1,j,k-\frac{1}{2}}(T_{1,j,k-1} - T_{1,j,k}) + K_{1,j,k+\frac{1}{2}}(T_{1,j,k+1} - T_{1,j,k}) \end{aligned} \quad (28)$$

The above two expressions for the unit cells are used to calculate the temperature change due to the cooling in time steps Δt for all cells, where the time step is limited by the stability criterion [7] in order to make the simulation stable.

This is obtained by writing equation 25 equivalently as:

$$P(t) = K_{eq}(T_{eq} - T_{i,j,k}(t)) \quad (29)$$

where K_{eq} is the equivalent heat conduction, T_{eq} is the equivalent surrounding temperature and $T_{i,j,k}(t)$ is the temperature in the cell of interest.

This gives a differential equation with the solution:

$$T_{i,j,k}(t) = T_{eq} + (T_0 - T_{eq})e^{-\frac{K_{eq}}{C_0}t} \quad (30)$$

where T_0 is the temperature in the cell of interest at time $t = 0$ and C_0 is the heat capacity of the cell.

In the numerical approach the heat flow is constant during a time step and is calculated at the beginning of each time step (here at $t = 0$). Hence, the temperature in the cell (i, j, k) follows the tangent of the analytical solution eq. 30 at $t = 0$.

It is impossible for the temperature $T_{i,j,k}(t)$ to be smaller than the surrounding temperature T_{eq}, which gives the following restriction on the time.

$$T_{eq} = -\frac{K_{eq}}{C_0}(T_0 - T_{eq}) \cdot t_{max} + T_0 \Rightarrow t_{max} = \frac{C_0}{K_{eq}} = \frac{C_0}{\sum K} \quad (31)$$

where

$$\sum K = K_{i-\frac{1}{2},j,k} + K_{i+\frac{1}{2},j,k} + K_{i,j-\frac{1}{2},k} + K_{i,j+\frac{1}{2},k} + K_{i,j,k-\frac{1}{2}} + K_{i,j,k+\frac{1}{2}} \quad (32)$$

Hence, the time step must be chosen within the interval $0 \leq t \leq t_{max}$ to give a stable numerical calculation. The criterion must be satisfied for all

cells and the smallest stable time step obtained is used for all cells. In this simulation $t_{max} = 0.002$ sec for all cells inside the block and $t_{max} = 0.005$ sec for cells with 3 facets facing the He gas. The time step is chosen to $\Delta t = 0.0005$ sec.

The temperature change for every time step is then:

$$\Delta T_{i,j,k} = \frac{P_{total(i,j,k)} \cdot \Delta t}{m \cdot c} \tag{33}$$

2.3.2. Diffusion of radionuclides in the tungsten block

The activity concentration inside the tungsten block depends on the production rate, the physical decay, the diffusion of the radionuclide and the transfer rate from surface to gas of the given radioelement. As an important example we have in the calculation below focused on hydrogen, or more specifically, tritium, H-3 because of its high production rate and suspected quantitative transfer from surface to cooling gas. However, the methodology developed can equally be utilized for other elements.

As an example we have used a production rate of $4.17{\cdot}10^6$ Bq/s reference?? for H-3 (total for all of target). An average specific production rate can then be calculated by dividing this number with the total volume of tungsten ($1\,\mathrm{m}^3$). This production rate is spatially distributed as the beam profile used previously.

Since we only look at activity release from the front block, we do not model the beam spreading further into the target. Thus the average H-3 production rate is assumed to be distributed in the front block as the beam profile, but maintaining the average (specific) production rate.

The physical decay of the radioisotopes are included in the finite element (finite time, finite volume) calculation, where the half-life for Tritium is taken as 12.3 years ($3.88 \cdot 10^8\,\mathrm{s}$) .

The migration of activity inside the target blocks is calculated on the basis of Fick's law acting on the activity concentration, where the concentration is the driving potential.

$$J = -D\nabla\phi \tag{34}$$

Here J is the diffusion flux (through an unit area) (Bq/s), D is the diffusion coefficient (m^2/s) and ϕ is the activity concentration of the radioisotope ($\mathrm{Bq/m}^3$).

As boundary condition we have taken the activity concentration to be zero in the gas phase, and thus assuming all radioelements falling over the

block surface are lost to the gas phase. The activity concentration in surface elements are not constantly zero - only in the gas.

No delay is introduced between activity arriving at the surface and its release to the gas phase. The diffusion coefficient depends strongly on temperature. We apply the Arrhenius equation for this:

$$D = D_0 \cdot \exp(\frac{-Q_D}{kT}) \tag{35}$$

where D_0 is the pre-exponential factor (m^2/s), Q_D is the activation energy (J), k is the Boltzmann constant $1.38 \cdot 10^{-23}$ J/K, and T is the absolute temperature (K).

The D_0 and Q_D values are global constants and do not depend on position inside the block. Our simulation has been carried out using $D_0 = 4.0 \cdot 10^{-7}$ m^2/s and $Q_D = 37650$ J/mol (for H-3)[9].

This temperature dependence corresponds to a factor of 2 in variation of the diffusion constant during one pulse cycle for a central block element. Thus the instantaneous diffusion speed inside the tungsten is varying by a factor 1.4 (because the diffusion length depends on $\sqrt{D}$).

The diffusion flux can now be found in the same way, as we calculated the energy flow rate (25).

$$\begin{aligned} J_{total(i,j,k)} = {} & F_{i-\frac{1}{2},j,k}(c_{i-1,j,k} - c_{i,j,k}) + F_{i+\frac{1}{2},j,k}(c_{i+1,j,k} - c_{i,j,k})... \\ & + F_{i,j-\frac{1}{2},k}(c_{i,j-1,k} - c_{i,j,k}) + F_{i,j+\frac{1}{2},k}(c_{i,j+1,k} - c_{i,j,k})... \\ & + F_{i,j,k-\frac{1}{2}}(c_{i,j,k+1} - c_{i,j,k}) + F_{i,j,k+\frac{1}{2}}(c_{i,j,k+1} - c_{i,j,k}) \end{aligned} \tag{36}$$

where $F_{i-\frac{1}{2},j,k}$ is the *diffusion conductance* between the two cells (i,j,k) and $(i-1,j,k)$ and is given by:

$$F_{i-\frac{1}{2},j,k} = \frac{\Delta y_j \Delta z_k}{\Delta x_i/(2D_{i,j,k}) + \Delta x_{i-1}/(2D_{i-1,j,k})} \tag{37}$$

The first term in the denominator is the *diffusion resistance* in the x-direction for half the cell (i,j,k) and the second term is the diffusion resistance for half the cell $(i-1,j,k)$.

For boundary cells, this expression is modified, e.g. for cell $(1,j,k)$:

$$F_{\frac{1}{2},j,k} = \frac{\Delta y_j \Delta z_k}{\Delta x_1/(2D_{1,j,k})} \tag{38}$$

Here we made the assumption that there is no resistance for isotopes arriving at the surface. Everything is removed by the gas and the concentration in the gas is set to 0.
The total diffusion from cell $(1, j, k)$ in the boundary layer is then:

$$\begin{aligned} J_{total(1,j,k)} = & F_{\frac{1}{2},j,k}(c_{He} - c_{1,j,k}) + F_{\frac{3}{2},j,k}(c_{2,j,k} - c_{1,j,k})... \\ & + F_{1,j-\frac{1}{2},k}(c_{1,j-1,k} - c_{1,j,k}) + F_{1,j+\frac{1}{2},k}(c_{1,j+1,k} - c_{1,j,k})... \\ & + F_{1,j,k-\frac{1}{2}}(c_{1,j,k+1} - c_{1,j,k}) + F_{1,j,k+\frac{1}{2}}(c_{1,j,k+1} - c_{1,j,k}) \end{aligned} \quad (39)$$

Now the change in the concentration for each cell is calculated in time steps Δt:

$$\Delta c_{i,j,k} = \frac{J_{total(i,j,k)} \cdot \Delta t}{\Delta x_i \cdot \Delta y_j \cdot \Delta z_k} \quad (40)$$

and added to the previously calculated concentration, which is multiplied by the exponential factor (of the decay law) in order to take the radioactive decay of the isotope into account.

The choice of time step for the thermal calculation does not necessarily coincide with the time step for the diffusion. Once the thermal behavior of the blocks is found as function of position and time, the diffusion behavior can be modeled in a coarser time resolution.

For this paper we were interested to see, if the pulse driven short-term variation in temperature (temperature peaks separated by one turn of the wheel (2.36 secs)) could possibly give rise to wave-like migration of the radionuclides, possibly accelerating the overall release.

Initial calculations on the temporal temperature variation allow the calculation of the range of diffusion constants encountered. Due to the limited temperature variation, the diffusion constants for any relevant radionuclide species in any block turn out to be almost constant (less than a factor of 2 in variation) during a wheel turn cycle.

The primary changes in diffusion constants happen during initial target warm-up that takes many tens of of revolutions. After steady state temperature is achieved, it can be seen that the differences in diffusion constants are much more dependent on position in the block (distance to surface) than on the time structure.

The duration of the beam pulse becomes unimportant for the diffusion simulation, and thus a much longer time step is chosen for diffusion simulation. We have used 10 msecs as time step in the diffusion simulation, which is far more detailed than necessary to capture the release behavior.

If a detailed calculation should be done, it can be carried our using the same formalism as above [7].

3. Results

Figure 4 shows the simulation of temperatures in centre cells of the (x, y), (y, z), (x, z) plans/facets and the centre cell of the block. The wheel rotation time structure is clearly shown with an amplitude of about 90°C at the center of the block. During the first several rotational cycles, the temperature in the tungsten builds up, until surface thermal transfer equals deposited beam power. During this the centre element temperature rises from 25°C to 525°C maximum.

From other calculations [5] we know that no other block sees a higher temperature or a higher temporal variation in temperature. The temperature results presented here are obtained based on a simple, first principles approach based only on beam profile and time structure, block geometry and the the surface heat transfer equation. Remarkably, we obtain the same maximum block temperature as a much more detailed full target simulation.

From the graph it is obvious that there are temperature gradients along the three axises, which give rise to very different diffusion coefficients throughout the tungsten block.

The fundamental result for a given radionuclide (for example H-3) is local concentration as a function of space and time. The activity concentrations as a function of time for typical front block elements are shown in figure 5, 7 and 8.

The total surface arrival rate of the tungsten block, and thus the total diffusion driven loss, can now be calculated by summing the flux over the total surface area. This result is seen in figure 9, which shows the cumulated activity concentration released at the block surface. In order to have the release in Bq, the values must be multiplied by the volume of the unit cell (10^{-9} m^3).

Based on this we can summarize the cumulative released activity and activity concentration (assuming a total gas phase distribution volume of $1m^3$), see figure 9.

The figure clearly shows that H-3 release is a slow process relative to the wheel revolution, but a very rapid process compared to the target operational periods of many months. Our time structure does not include simulation of

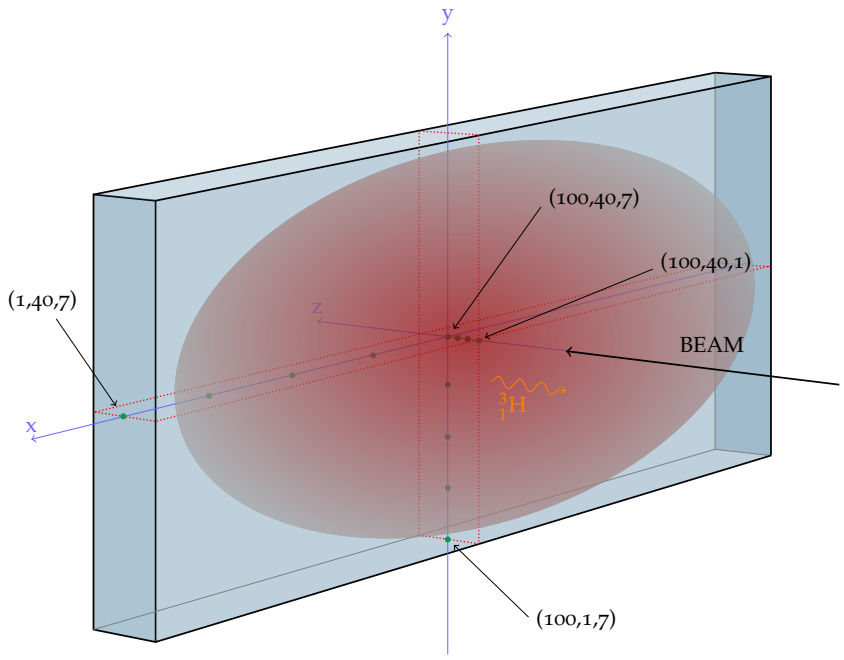

Figure 3: The figure shows the points of simulation for both the temperature and the activity concentration. All sides of the block are cooled by helium and the foot print of the beam is indicated on the front surface. The foot print actually covers the total surface area, but the intensity increases towards the centre of the beam. The diffusion of H-3 mainly takes place in the z-direction along the hottest paths through the two largest surfaces.

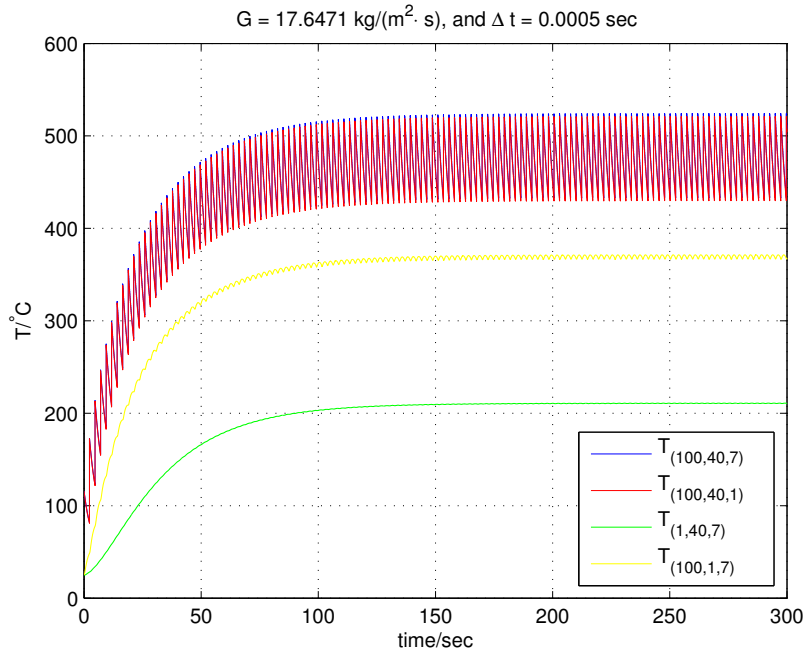

Figure 4: The graph shows the temperature profile for different centre cells of the tungsten block over time.

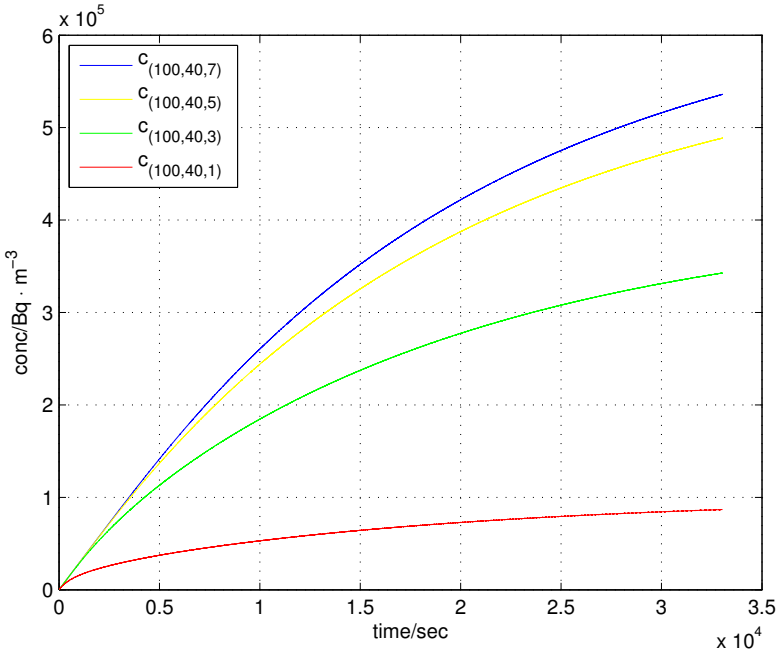

Figure 5: Concentrations profiles of H-3 in tungsten along the centre axis through the (x,y) facet.

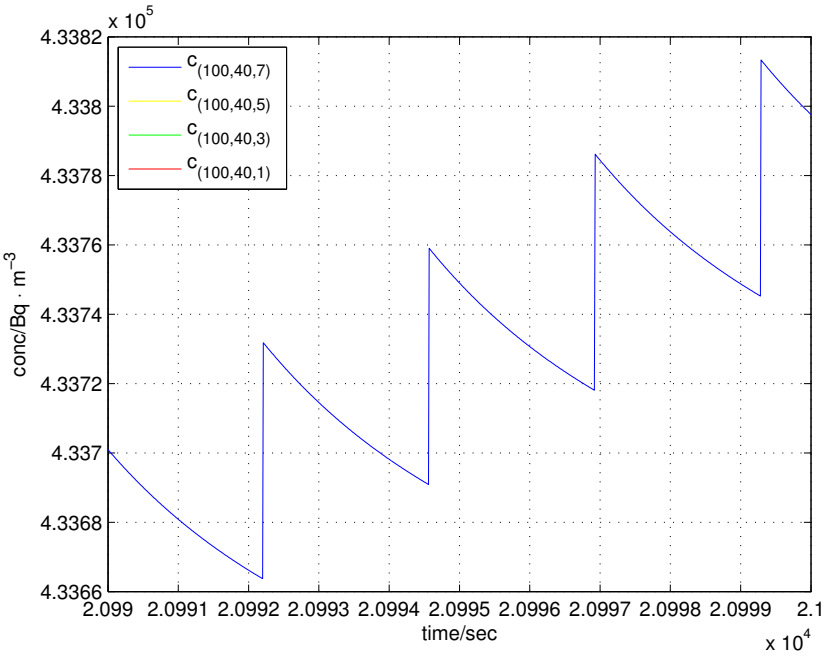

Figure 6: Perhaps this figure should be deleted Zoom of the blue line (block centre) in figure 5 to see the temporal structure of the activity concentration. Zoom is taken approximately 6 hours after first beam on.

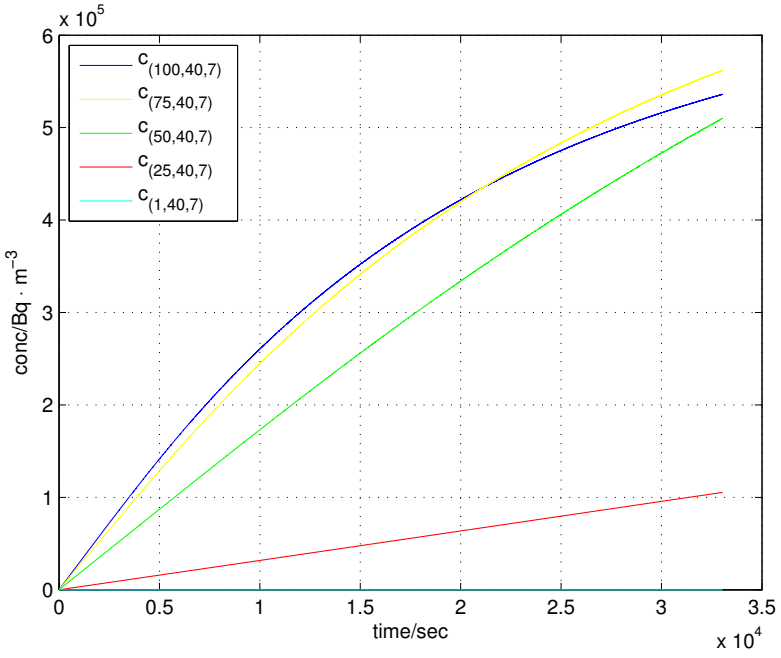

Figure 7: Concentrations profiles of H-3 in tungsten along the centre axis through the (y,z) facet.

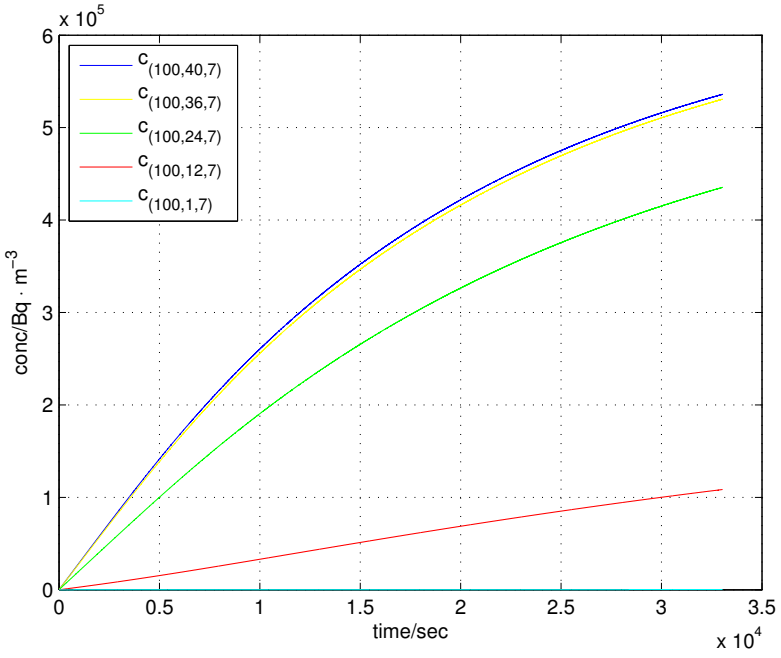

Figure 8: Concentrations profiles of H-3 in tungsten along the centre axis through the (x,z) facet.

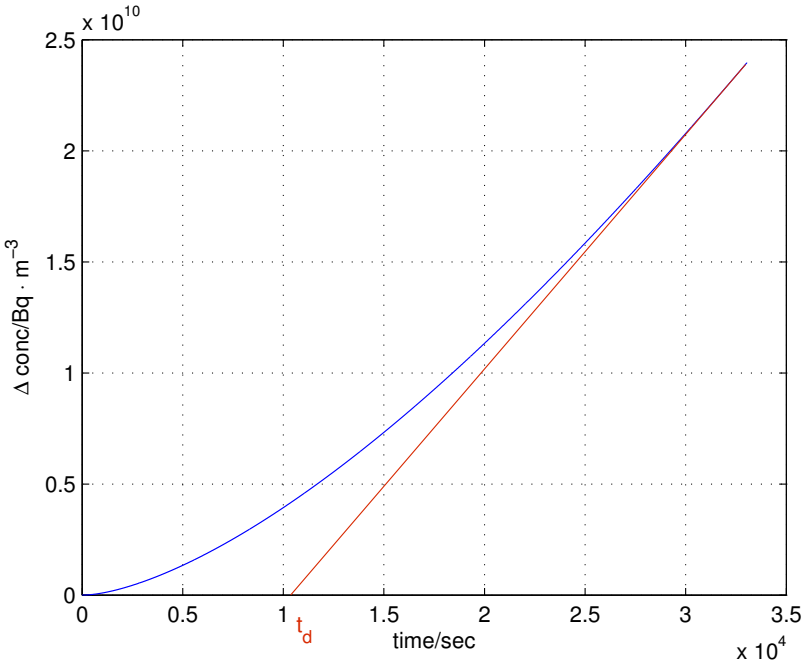

Figure 9: Cumulated H-3 removal from the overall surface of the tungsten block. The removal in Bq is found by multiplying all values (ordinates) by the volume of a unit cell (10^{-9} m^3). t_d is found to be $1.0 \cdot 10^4$ secs, but since steady state has not occurred, the actual value of t_d is a little higher.

beam off periods, but the main outcomes are that the H-3 release is total, but happens with a delay in the order of hours.

As the production rate in the target is constant during beam on, the released activity over time asymptotically approaches the total production, and that is linear increase over time. Extending this asymptotic line to zero crossing gives the time at which 1/e of the produced activity has escaped, and that is the same as t_d. The value of t_d is in this case $1.0 \cdot 10^4$ secs, but since steady state is not achieved, the actual t_d is a little higher. This value is important, as it allows for comparison with the rate calculated by the analytical solution.

Figure 10 shows the relationship between the temperature of the block and t_d (from the analytical solution), and it is seen from the graph that $t_d = 1.0 \cdot 10^4$ secs gives a temperature of 525°C, which agrees with the maximum temperature of the core cells in the numerical calculation.

Hence, this substantiates the equivalence between the analytical and the numerical solution.

4. Discussion

The results of the thermal simulation are only of importance to set the framework for the diffusion calculation. For this we needed to understand something that is not contained in the present baseline calculations, that is the detailed time structure of the temperature inside a given block.

However, our calculation shows that the pulse variation is always lower than 100 degrees. Of course this has a different impact depending on the diffusing element in question. However, even for the most mobile species considered (Hydrogen/Tritium) this gives an insignificant variation in the diffusion length encountered during a rotation period.

Thus it is only the spatial variation in temperature that needs to be considered in the release calculation. The detailed time structure of the diffusion can be ignored safely, and the overall release rate can be analyzed in the terms of the steady state temperature spatial distribution.

As the heat up of the wheel after beam on is fast compared to the average diffusion time (for all radionuclides considered), our results prove that the release calculation can even be reduced to a calculation of an average, steady state diffusion delay (or activity hold-up time) that only depends on the spatial variation of temperature inside the block.

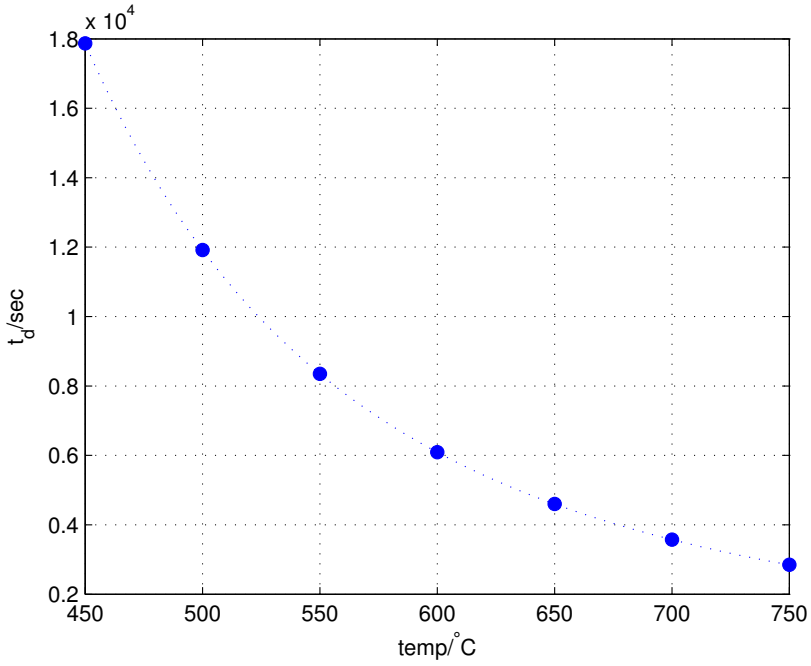

Figure 10: The graph shows the typical time, t_d for release of a given species of activity as a function of temperature (analytical solution).

Said more precisely, we have found that there is a *typical* temperature T_d for a given block showing a core temperature T_{max} and a surface temperature T_{min} with $T_{min} < T_d < T_{max}$ that can be used for insertion into the Arrhenius equation to calculate the diffusion constant.

Due to the highly anisotropic geometry of the tungsten blocks, and most importantly the release dominating front blocks, the spatial variation of the temperature is almost independent of the position in the beam direction - should be moved up in the text (the z-direction, as demonstrated in figure 4). The z-direction is however also by far the nearest route to the surface from the block centre, and the total diffusion rate will be completely dominated by the temperature along this route.

The variation here is small, and thus these results lead to the conclusion that the analytical solution to the activity transport and release can be used safely for a given block by applying a diffusion constant derived from the maximum temperature, that is the *core* temperature T_{max} of the block.

Furthermore, we can safely apply the time averaged temperature of this core element in the calculations. In the end we conclude that:

1. The radioactive release rate for a given radioactive species is governed by the production rate reduced by a decay loss in the order of $t_d/t_{1/2}$.
2. This behavior is well described by the analytical solution that is based on the Fourier expansion.
3. The diffusion constant to be used is safely calculated by using the Arrhenius equation with $T = T_{max}$.

5. Conclusion

The above conclusions may seem simple and intuitive once stated. However, we have derived the approximation based on detailed numerical simulations. It has guided us to the conclusion that the overall target release can be based on considerations of a single dominating block (the foremost) with a production rate equal to the overall target production rate. The warm-up period of the target wheel is insignificant compared to the release delay, and thus it is only the steady state diffusion that needs consideration.

6. References

[1] International Atomic Energy Agency, Nuclear Technology Review 2012

[2] D.A. McClintock, B.W. Riemer, P.D. Ferguson, A.J. Carroll, M.J. Dayton, Initial observations of cavitation-induced erosion of liquid metal spallation target vessel at the Spallation Neutron Source, Journal of Nuclear Materials 431 (2012) 147-159.

[3] B.W. Riemer, D.A. McClintock, S. Kaminskas, A.A. Abdou, Correlation between simulations and cavitation-induced erosion damage in Spallation Neutron Source target modules after operation, Journal of Nuclear Materials 450 (2014) 183191.

[4] Target Station Design Update Baseline, December 2011

[5] Heat Deposition in Tungsten Target, ESS Target Design Review Report, 1164465, v.2

[6] Samuel Glasstone, Alexander Sesonske, Nuclear Reactor Engineering, 1963, Van Nostrand, (p. 365-371)

[7] Bengt Eftring, Numerisk beräkning av temperaturförlopp. Numerical calculations of thermal processes (written in swedish), 1990, Byggforskningsrådet, The Swedish Council for Building Research, Report R81:1990

[8] Thomas Blomberg, Heat Conduction in Two and Three Dimensions, May 1996, Dep. of Building Physics, Lund University, Sweden

[9] R. Fraunfelder, J. Vac. Sci. Technol. 6, 388 (1969); doi: 10.1116/1.1492699